



Contents lists available at ScienceDirect

Journal of Quantitative Spectroscopy & Radiative Transfer

journal homepage: www.elsevier.com/locate/jqsrt

Light scattering by an erythrocyte based on discrete sources method: Shape and refractive index influence

Elena Eremina *

University of Bremen, Badgasteiner Street 3, 28359 Bremen, Germany

ARTICLE INFO

Article history:

Received 20 November 2008

Received in revised form

26 January 2009

Accepted 4 March 2009

Keywords:

Red blood cell

Light scattering

Discrete sources method

ABSTRACT

An efficient method for the fast detection of properties of a single erythrocyte from its scattering characteristics is needed in practice. To develop such a method a detailed investigation of the light scattering properties of the erythrocyte and their dependence on its shape and refractive index is of great interest. In this paper the influence of the real erythrocyte's shape with deep concavities and refractive index on the scattering characteristics is analyzed based on an updated scheme of the discrete sources method. Realistic shape models of an erythrocyte, calculated from minima of membrane potential energy are considered. The numerical scheme of discrete sources method has been adjusted for shape profiles given numerically. An improved algorithm allows increasing of an accuracy of calculations.

© 2009 Elsevier Ltd. All rights reserved.

1. Introduction

Light scattering by human blood cells is of great interest in different practical applications, due to the important role they play in our body. In particular, the measurement of light scattering by blood cells is a suitable method for investigation of blood cells properties: shape, size and refractive index, which can serve as markers for different human diseases [1]. The investigation of properties of a red blood cell (erythrocyte) and their connection to the scattered light is in focus of interest for years now, especially in modeling applications [2–4]. The reason is that change of erythrocyte's physical properties, like shape or hemoglobin content can be used for detection of diseases. The problem of reconstruction of erythrocyte's properties from its light scattering characteristics is an inverse scattering problem [5]. In nature the shape of a human erythrocyte can vary in from nearly spherical through biconcave to toroidal ones and the refractive index of the cell depends on its hemoglobin concentration. These aspects complicate modeling and make the inverse problem hard to solve [6].

On one hand, the modeling of light scattering by an erythrocyte should not be complicated as the particle demonstrates no internal structure, on the other hand its large size (typically in the range of 6–10 μm) and complicated shape of healthy erythrocyte (biconcave discoid) causes problems which can not be overcome by many modeling methods.

During the recent years different simulation methods have been applied to model light scattering by erythrocyte: finite difference time domain (FDTD) [7], discrete dipole approximation (DDA) [8], multipole multiple technique (MMP), *T*-matrix method [9], null-field method with discrete sources (NFM-DS) [3], discrete sources method (DSM) [4,10] and some others.

Another problem for modeling is to find an appropriate shape model of an erythrocyte which reproduces a real shape. In the last years different shape approaches have been suggested to model the erythrocyte: from simple spherical to more

* Tel.: +49 421 218 3583; fax: +49 421 218 5378.

E-mail address: eremina@iwt.uni-bremen.de

complicated artificial models, trying to approach a real biconcave shape of an erythrocyte. The most realistic biconcave models were suggested by Fung et al. [11] and Skalak [12]. Another attempt was based on Cassini ovals [3]. Recently there is a new method to find the shape of biological particles from the condition of minima of membrane potential energy [13]. An erythrocyte shape profiles are calculated for given volume and surface area by means of the surface evolver code.

In this paper the DSM [14] is adjusted to model the light scattering by several of such profiles. The main goal was an estimation of the influence of erythrocyte shape and the refractive index on light scattering characteristics. By using of such models like Fung, Skalak or Cassini-based model, which are given analytically, it was possible to deposit the discrete sources (DS) inside the scatterer analytically as well. In contrast to analytical shapes, the shape profiles discussed in this paper are given numerically. To adjust the DSM algorithm for numerically given shapes and to provide the stability of calculation results, the DSM model has been improved. In particular, vector potentials based on spherical Hankel functions have been chosen for the field’s representation inside the particle. This circumstance allowed accounting for deep concavities of an erythrocyte shape.

The second part of the paper describes the theoretical basement of the DSM followed by the numerical algorithm and modeling results.

2. Theory

Let us consider scattering in an isotropic homogeneous medium in R^3 of an electromagnetic wave by a local homogeneous penetrable obstacle D_i with a smooth boundary ∂D . We use a cylindrical coordinate system (z, θ, φ) , where z is also the axis of symmetry of a particle. As an external excitation we will consider a plane wave with an incident angle $\pi - \theta_0$ with respect to the z -axis. Then the mathematical statement of the scattering problem can be formulated as follows:

$$\begin{aligned} \nabla \times \mathbf{H}_{e,i} &= jk\varepsilon_{e,i}\mathbf{E}_{e,i}; \quad \nabla \times \mathbf{E}_{e,i} = -jk\mu_{e,i}\mathbf{H}_{e,i} \quad \text{in } D_{e,i}, \quad D_e := R^3 / \overline{D_i}; \\ \mathbf{n}_p \times (\mathbf{E}_i(P) - \mathbf{E}_e(P)) &= \mathbf{n}_p \times \mathbf{E}^0(P), \\ \mathbf{n}_p \times (\mathbf{H}_i(P) - \mathbf{H}_e(P)) &= \mathbf{n}_p \times \mathbf{H}^0(P), \quad P \in \partial D \end{aligned} \tag{1}$$

and the Silver–Muller radiation condition at infinity.

Here $\{\mathbf{E}^0, \mathbf{H}^0\}$ is the exciting field, $\{\mathbf{E}_i, \mathbf{H}_i\}$ is the total field inside the particle and $\{\mathbf{E}_e, \mathbf{H}_e\}$ is the scattered field. \mathbf{n}_p is the unit outward normal to ∂D , index e belongs to the external domain $D_{e,i}$ —to the domain inside the particle D_i , $\text{Im } \varepsilon_e, \mu_e = 0$ and $\text{Im } \varepsilon_i, \mu_i \leq 0$. We assume the time dependence to be chosen as $\exp\{j\omega t\}$. Then the boundary value scattering problem (1) has the unique solution [15].

One of the most attractive features of the DSM consists in a flexible choice of the fields of the DS which can be used to construct an approximate solution. Additionally, there are no limitations to a choice of support of the DS. The last ones should provide fulfilling Maxwell equations, radiation conditions and present a complete system of fields at the obstacle surface [14].

We will consider an axial symmetric particle. In this case the system of the lowest order multipoles distributed over the axis of symmetry can be applied to construct an approximate solution [16]. We will construct the approximate solution by taking into account not only the rotational symmetry of the obstacle, but the polarization of an external excitation as well. In case of a P -polarized exciting plane wave the exciting field accepts the following form:

$$\begin{aligned} \mathbf{E}^0 &= (\mathbf{e}_x \cos \theta_0 + \mathbf{e}_z \sin \theta_0) \exp\{-jk_e(x \sin \theta_0 - z \cos \theta_0)\}, \\ \mathbf{H}^0 &= -\mathbf{e}_y \cos \theta_0 n_0 \exp\{-jk_e(x \sin \theta_0 - z \cos \theta_0)\}, \end{aligned} \tag{2}$$

where $k_e = k\sqrt{\varepsilon_e \mu_e}$.

Implementing plane wave resolution, one gets

$$\exp\{\pm jv \cos \varphi\} = \sum_{m=0}^{\infty} (2 - \delta_{0m})(\pm j)^m J_m(v) \cos m\varphi,$$

where J_m is the cylindrical Bessel function and δ_{0m} is the Kronecker symbol.

The Fourier harmonics for the external excitation in a cylindrical coordinate system can be written as

$$\begin{aligned} \mathbf{E}_m^0 &= \{\mathbf{E}_{m\rho}^{0,P}(\eta) \cos(m+1)\varphi; \mathbf{E}_{m\rho}^{0,P}(\eta) \sin(m+1)\varphi; \mathbf{E}_{mz}^{0,P}(\eta) \cos(m+1)\varphi\}, \\ \mathbf{H}_m^0 &= \{\mathbf{H}_{m\rho}^{0,P}(\eta) \sin(m+1)\varphi; \mathbf{H}_{m\rho}^{0,P}(\eta) \cos(m+1)\varphi; \mathbf{H}_{mz}^{0,P}(\eta) \sin(m+1)\varphi\}. \end{aligned}$$

To take the polarization of the external excitation into account, we use some linear combination of electrical and magnetic multipoles. For this we need special vector potentials. In case of P -polarization of the plane wave the vector

potentials in a cylindrical coordinate system can be represented as

$$\begin{aligned} \mathbf{A}_{mn}^{1,e,i} &= \{Y_m^{e,i}(\eta, w_n^{e,i}) \cos(m+1)\varphi; -Y_m^{e,i}(\eta, w_n^{e,i}) \sin(m+1)\varphi; 0\}, \\ \mathbf{A}_{mn}^{2,e,i} &= \{Y_m^{e,i}(\eta, w_n^{e,i}) \sin(m+1)\varphi; Y_m^{e,i}(\eta, w_n^{e,i}) \cos(m+1)\varphi; 0\}, \\ \mathbf{A}_n^{3,e,i} &= \{0; 0; Y_0^{e,i}(\eta, w_n^{e,i})\}. \end{aligned} \tag{3}$$

Here $Y_m^e(\eta, w_n^e) = h_m^{(2)}(k_e R_{\eta w_n^e})(\rho/R_{\eta w_n^e})^m$, $Y_m^i(\eta, w_n^i) = h_m^{(2)}(k_i R_{\eta w_n^i})(\rho/R_{\eta w_n^i})^m$, $R_{\eta w_n^{e,i}}^2 = \rho^2 + (z - w_n^{e,i})^2$, $\eta = (\rho, z)$, $h_m^{(2)}$ are spherical Hankel functions and $w_n^{e,i}$ are complex coordinates of the DS in an adjoined complex plane so, that $\text{Re}(w_n^e) \in D_i$ and $\text{Re}(w_n^i) \in D_e$. Such presentation based on just spherical Hankel functions in contrast to those used in [10] provides an improved stability of numerical scheme and increases an accuracy of calculations, especially in the side-scattering direction. This fact seems to be especially import for calculation of real erythrocyte's shape with deep concavities.

According to the details mentioned above the approximate solution for *P*-polarization of the plane wave accepts the following form:

$$\begin{aligned} \mathbf{E}_{e,i}^N &= \sum_{m=0}^M \sum_{n=1}^{N_{e,i}^m} \left\{ p_{mn}^{e,i} \frac{j}{k \varepsilon_{e,i} \mu_{e,i}} \nabla \times \nabla \times \mathbf{A}_{mn}^{1,e,i} + q_{mn}^{e,i} \frac{j}{\varepsilon_{e,i}} \nabla \times \mathbf{A}_{mn}^{2,e,i} \right\} + \sum_{n=1}^{N_{e,i}^0} r_n^{e,i} \frac{j}{k \varepsilon_{e,i} \mu_{e,i}} \nabla \times \nabla \times \mathbf{A}_n^{3,e,i}, \\ \mathbf{H}_{e,i}^N &= \frac{j}{k \mu_e} \nabla \times \mathbf{E}_{e,i}^N \end{aligned} \tag{4}$$

For *S*-polarization of the exciting plane wave the exciting field accepts the following form:

$$\begin{aligned} \mathbf{E}^0 &= \mathbf{e}_y \cos \theta_0 \exp\{-jk_e(x \sin \theta_0 - z \cos \theta_0)\}, \\ \mathbf{H}^0 &= (\mathbf{e}_x \cos \theta_0 + \mathbf{e}_z \sin \theta_0) n_0 \exp\{-jk_e(x \sin \theta_0 - z \cos \theta_0)\}. \end{aligned}$$

The Fourier harmonics for the external excitation can be written as

$$\begin{aligned} \mathbf{E}_m^0 &= \{\mathbf{E}_{m\rho}^{0,S}(\eta) \sin(m+1)\varphi; \mathbf{E}_{m\rho}^{0,S}(\eta) \cos(m+1)\varphi; \mathbf{E}_{mz}^{0,S}(\eta) \sin(m+1)\varphi\}, \\ \mathbf{H}_m^0 &= \{\mathbf{H}_{m\rho}^{0,S}(\eta) \cos(m+1)\varphi; \mathbf{H}_{m\rho}^{0,S}(\eta) \sin(m+1)\varphi; \mathbf{H}_{mz}^{0,S}(\eta) \cos(m+1)\varphi\}. \end{aligned}$$

Then the approximate solution for the *S*-polarized exciting plane wave takes a form:

$$\begin{aligned} \mathbf{E}_{e,i}^N &= \sum_{m=0}^M \sum_{n=1}^{N_{e,i}^m} \left\{ p_{mn}^{e,i} \frac{j}{k \varepsilon_{e,i} \mu_{e,i}} \nabla \times \nabla \times \mathbf{A}_{mn}^{1,e,i} + q_{mn}^{e,i} \frac{j}{\varepsilon_{e,i}} \nabla \times \mathbf{A}_{mn}^{2,e,i} \right\} + \sum_{n=1}^{N_{e,i}^0} r_n^{e,i} \frac{j}{\varepsilon_{e,i}} \nabla \times \mathbf{A}_n^{3,e,i}, \\ \mathbf{H}_{e,i}^N &= \frac{j}{k \mu_e} \nabla \times \mathbf{E}_{e,i}^N, \end{aligned} \tag{5}$$

where the vector potentials accept following expressions:

$$\begin{aligned} \mathbf{A}_{mn}^{1,e,i} &= \{Y_m^{e,i}(\eta, w_n^{e,i}) \sin(m+1)\varphi; Y_m^{e,i}(\eta, w_n^{e,i}) \cos(m+1)\varphi; 0\}, \\ \mathbf{A}_{mn}^{2,e,i} &= \{Y_m^{e,i}(\eta, w_n^{e,i}) \cos(m+1)\varphi; -Y_m^{e,i}(\eta, w_n^{e,i}) \sin(m+1)\varphi; 0\}, \\ \mathbf{A}_n^{3,e,i} &= \{0; 0; Y_0^{e,i}(\eta, w_n^{e,i})\}. \end{aligned} \tag{6}$$

The completeness of the system of lowest-order distributed multipoles used in (3) and (6) guarantees the convergence of the approximate solution (4) and (5) to the exact one in any closed subset of D_e [16].

3. Numerical scheme of DSM

Let us now describe the computational algorithm in details. As we outlined above the representations (4, 5) satisfy all the conditions of the scattering problem (1) except the transmission conditions at the particle surface. These last conditions are used to determine the unknown amplitudes of DS $\{p_{mn}^{e,i}, q_{mn}^{e,i}, r_n^{e,i}\}$. Since the scattering problem geometry is axially symmetric with respect to the *z*-axis representations for the scattered and total fields (4, 5) accept the form of a finite sum of a Fourier series with respect to φ . Besides, the exciting field can also be resolved into Fourier series. This means that fulfilling the transmission conditions at the surface ∂D can be reduced to a sequential solution of the 1D transmission problems for the Fourier harmonics of the fields. So, instead of matching the fields on the scattering surface, we can match their Fourier harmonics separately thus reducing the approximation problem on the surface ∂D to a set of 1D problems enforced at the particle generatrix. By solving these problems one can determine the required DS amplitudes $\{p_{mn}^{e,i}, q_{mn}^{e,i}, r_n^{e,i}\}$.

Various numerical schemes for the amplitudes evaluation have been suggested. It has been found that the most stable results can be obtained by using the generalized point-matching technique and a pseudo-solution of the associated over-determined system of linear equations [17]. As DSM is a direct method, it allows solving the scattering problem for the entire set of incident angles $(\pi - \theta_0)$ and for both polarizations (*P* and *S*) at once. This is an advantage compared to methods which incorporate an iterative scheme for the linear system solution. Besides, the DSM numerical scheme provides an

opportunity to control the actual convergence of the approximate solution to the exact one by a-posterior evaluating of surface residual [16].

We use an extended version of the DSM algorithm described by Eremin [14]. For oblate obstacles it can be necessary to deposit the DS in a complex plane [4]. Such a procedure allows to limit the DS sequence, when $N \rightarrow \infty$. The limitation is very important to provide the stability of the numerical model based on DSM.

Therefore the different numbers of DS for the representation of the scattered field outside and total field inside the particle are used. The numbers of DS are chosen proportionally to the value of refractive index of the corresponding media.

For the estimation of the real accuracy of the computational results, the convergence test is done in two steps:

1. Controlling of the internal convergence of the results by increasing the number of matching points and DS.
2. Evaluating the surface residual in least square norm.

The achieved residual provides stabilization of the scattering diagram at the second digit after decimal point. The required number of matching points is reached by increasing the number until the necessary accuracy of the results is achieved. The DS number usually is 2–4 times less than the number of the matching points. The order of multipoles (M) is a priori defined from the condition that the plane wave approximation by corresponding Fourier series should be less then 0.2%.

After the amplitudes of the DS are determined, one can calculate the far field pattern $\mathbf{F}(\theta, \varphi)$ of the scattered field, which is determined at the upper part of the unite semi-sphere $\Omega = \{0^\circ \leq \theta \leq 90^\circ, 0^\circ \leq \phi \leq 360^\circ\}$ and is given by

$$\mathbf{E}_e(\mathbf{r})/|\mathbf{E}^0(\mathbf{r})| = \frac{\exp\{-jk_e r\}}{r} \mathbf{F}(\theta, \varphi) + O(1/r^2), \quad r \rightarrow \infty, z > 0.$$

Using an asymptotic representation for $Y_m^{e,i}$ for a P-polarized exciting plane wave, the following representation for the θ, φ -components of the far field pattern corresponding to representation (4) accepts the form:

$$\begin{aligned} F_\theta^P(\theta, \varphi) &= j \sum_{m=0}^M (j \sin \theta)^m \cos(m+1)\varphi \sum_{n=1}^{N_e^m} \{p_{mn}^e \cos \theta + q_{nm}^e\} \exp\{-jk_e z_n \cos \theta\} \\ &\quad - j \sin \theta \sum_{n=1}^{N_e^0} r_n^e \exp\{-jk_e z_n \cos \theta\}, \\ F_\varphi^P(\theta, \varphi) &= -j \sum_{m=0}^M (j \sin \theta)^m \sin(m+1)\varphi \sum_{n=1}^{N_e^m} \{p_{mn}^e + q_{nm}^e \cos \theta\} \exp\{-jk_e z_n \cos \theta\}. \end{aligned} \tag{7}$$

For S-polarized excitation following representations are valid for components of the far field pattern involved into (5):

$$\begin{aligned} F_\theta^S(\theta, \varphi) &= j \sum_{m=0}^M (j \sin \theta)^m \sin(m+1)\varphi \sum_{n=1}^{N_e^m} \{p_{mn}^e \cos \theta - q_{nm}^e\} \exp\{-jk_e z_n \cos \theta\}, \\ F_\varphi^S(\theta, \varphi) &= j \sum_{m=0}^M (j \sin \theta)^m \cos(m+1)\varphi \sum_{n=1}^{N_e^m} \{p_{mn}^e - q_{nm}^e \cos \theta\} \exp\{-jk_e z_n \cos \theta\} \\ &\quad + j \sin \theta \sum_{n=1}^{N_e^0} r_n^e \exp\{-jk_e z_n \cos \theta\}. \end{aligned} \tag{8}$$

After the unknown amplitudes of the DS are determined, the far field patterns for P and S polarizations are represented as finite linear combinations of elementary functions. This fact ensures low computational efforts for the analysis of the scattering characteristics in the far zone.

The intensity of scattered light can be calculated as follows

$$I^{P,S}(\theta_0, \theta, \varphi) = |F_\theta^{P,S}(\theta_0, \theta, \varphi)|^2 + |F_\varphi^{P,S}(\theta_0, \theta, \varphi)|^2,$$

where $F_{\theta,\varphi}^{P,S}(\theta_0, \theta, \varphi)$ are the components of the far field pattern for P (4) and S (5) polarized incident waves, in a spherical coordinate system θ, φ . In this paper the intensity of unpolarized scattered light is discussed:

$$I(\theta_0, \theta, \varphi) = \frac{1}{2}(I^P(\theta_0, \theta, \varphi) + I^S(\theta_0, \theta, \varphi)). \tag{9}$$

4. Numerical results and discussion

In this part selected numerical results will be presented. In flow cytometry model suggested by Maltsev [6,18] for erythrocyte studies a red laser with a wavelength of $\lambda = 0.632 \mu\text{m}$ is used. Blood cells are usually investigated in water with

refractive index $n = 1.33$, so the relative incident wavelength used for modeling was taken: $\lambda = 0.494 \mu\text{m}$. Typical human erythrocyte has a size of $6\text{--}9 \mu\text{m}$ and a relative refractive index in the range of $1.0355\text{--}1.0596$. For modeling three different shapes obtained by the surface evolver code have been taken. The surface evolver code enables to obtain the shape of erythrocyte for certain surface area and volume from the condition of minima of the membrane potential energy. The code is free for use and can be downloaded from the internet [19]. In contrast to analytical erythrocyte shapes the shape profiles calculated with surface evolver are given numerically. For convenience of comparison three shapes with different volume and surface area, but the same diameter $D = 6.32 \mu\text{m}$ have been used. Detailed parameters are presented in Table 1 and the shape forms are depicted in Fig. 1.

In the model used in the paper the incident plane wave falls in zx -plane and the wave vector k belongs to the plane $\varphi = 0$. Because of this the maximum of the diagram's values (forward scattering) belongs to the plane $\varphi = 180$, which formally corresponds to the negative values of θ angle. Due to this fact in the diagrams presented below values of scattering angle θ are negative.

Table 1

Parameters of erythrocyte's profiles.

Shape	Volume (μm^3)	Area (μm^2)	Sphericity index
V3	50	90	0.622777
V2	64.63	93.15	0.764515
V1	81.87	99.61	0.875783

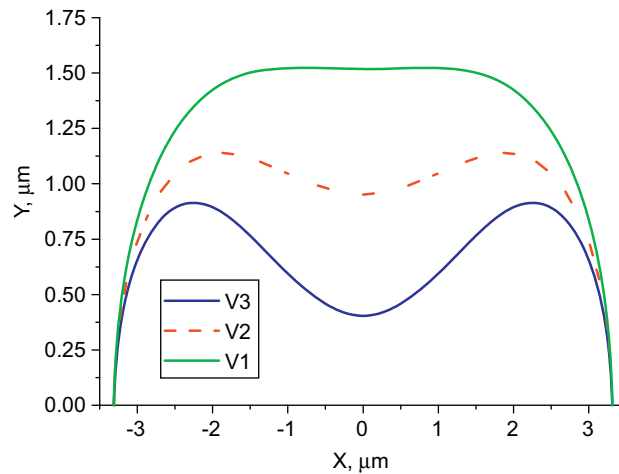


Fig. 1. Profiles of different erythrocyte shapes used for light scattering simulations. Diameter $D = 6.32 \mu\text{m}$.

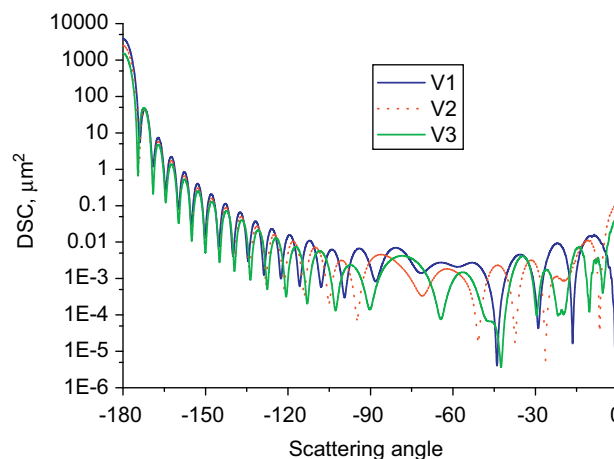


Fig. 2. Intensity of unpolarized scattered light (9) (scattering diagram) for different erythrocyte shapes: V1–V3. Incident angle $\theta_0 = 0^\circ$.

Let us now discuss some exemplary numerical results. In Fig. 2 the scattering diagram of unpolarized light (9) is presented for the different erythrocyte shapes V1–V3, under the incident angle $\theta_0 = 0^\circ$ (parallel to the symmetry axis of the erythrocyte). The refractive index was fixed at $n = 1.047$ and the residual of calculation results did not exceed 0.6%.

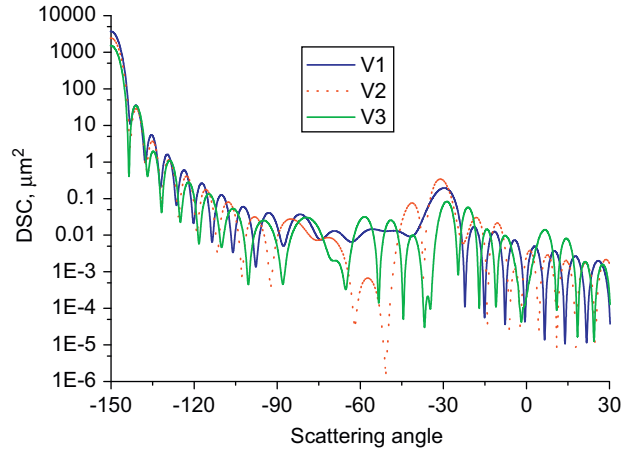


Fig. 3. Scattering diagram for different erythrocyte shapes. $\theta_0 = 30^\circ$.

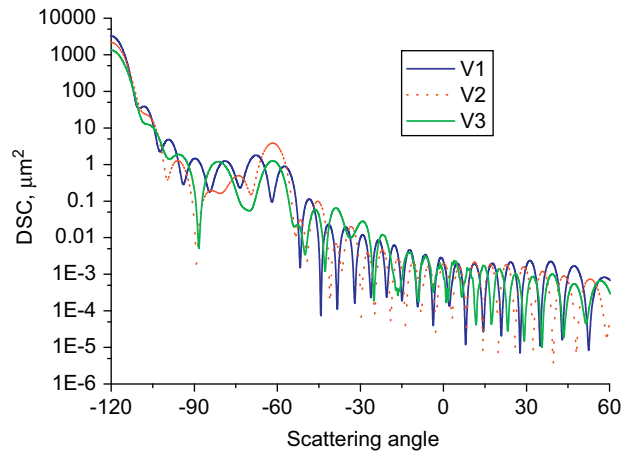


Fig. 4. Scattering diagram for different erythrocyte shapes. $\theta_0 = 60^\circ$.

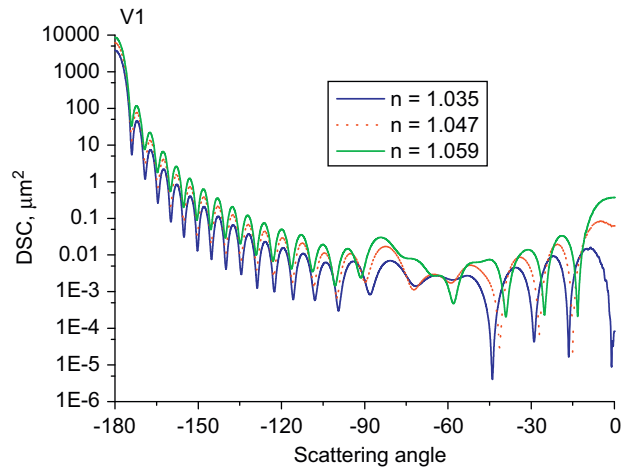


Fig. 5. Scattering diagrams for erythrocyte shape V1 for difference refractive indices. $\theta_0 = 0^\circ$.

In Figs. 3 and 4 corresponding results are presented for incident angles $\theta_0 = 30^\circ$ and 60° , respectively (max. residual for both incident angles 0.2%). Note that in all presented figures the x-axis is adjusted starting with the forward scattering direction for the convenience of comparison. From the results one can see, that the difference in the curves is more

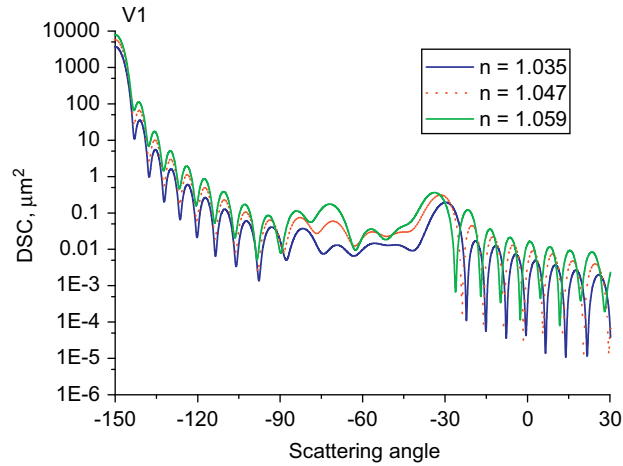


Fig. 6. Scattering diagrams for erythrocyte shape V1 for difference refractive indices. $\theta_0 = 30^\circ$.

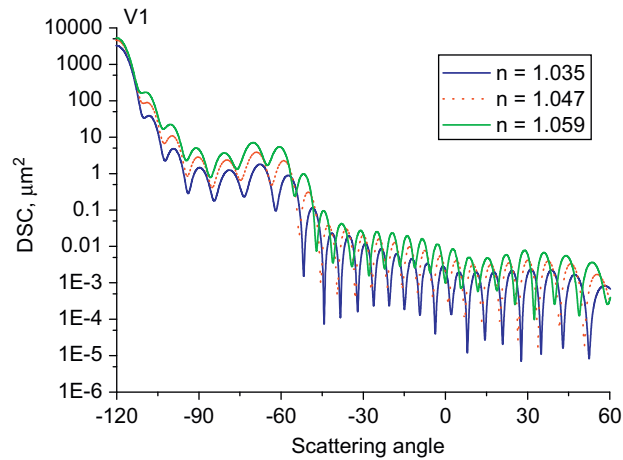


Fig. 7. Scattering diagrams for erythrocyte shape V1 for difference refractive indices. $\theta_0 = 60^\circ$.

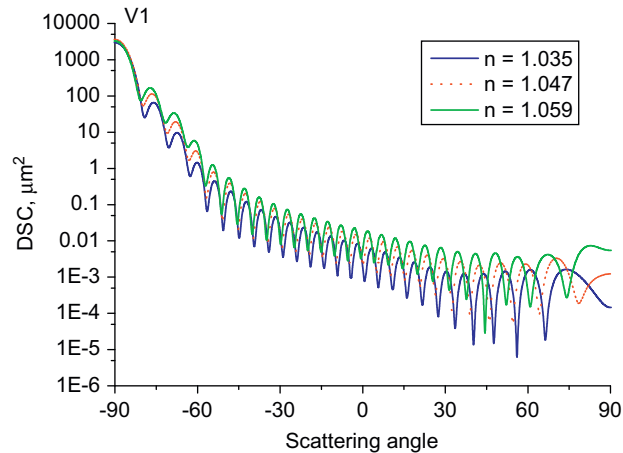


Fig. 8. Scattering diagrams for erythrocyte shape V1 for difference refractive indices. $\theta_0 = 90^\circ$.

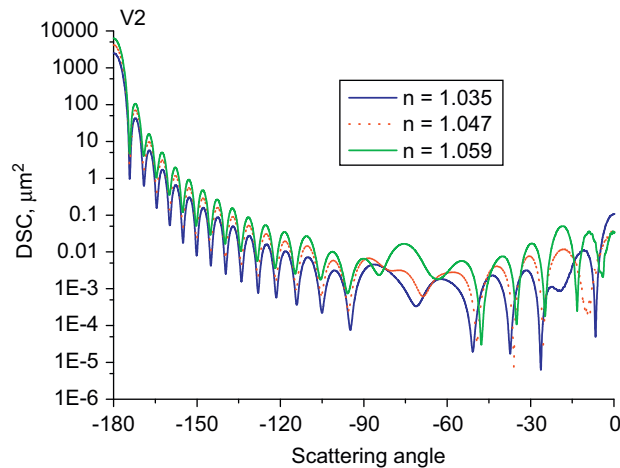


Fig. 9. Scattering diagrams for erythrocyte shape V2 for difference refractive indices. $\theta_0 = 0^\circ$.

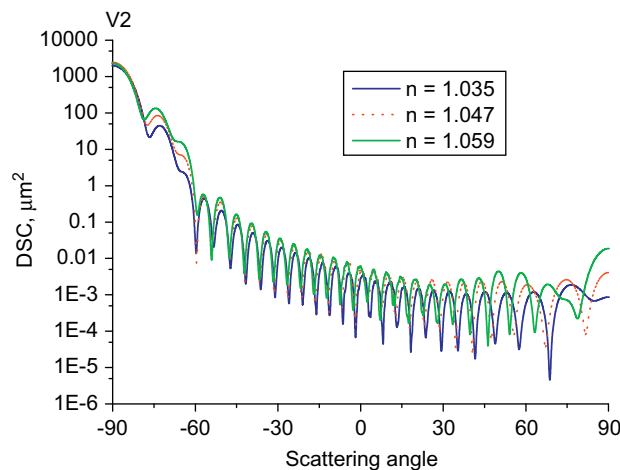


Fig. 10. Scattering diagrams for erythrocyte shape V2 for difference refractive indices. $\theta_0 = 90^\circ$.

pronounced in side- and backscattering directions and gets more obvious with the increasing values for the incident angle. While for the $\theta_0 = 0^\circ$ the difference between the curves is more pronounced in the back scattering direction, for the incidence of 30° and 60° this area shifts closer to the main scattering direction.

Now let us investigate the dependence of the scattered intensity on the refractive index. For this purpose three different values of refractive index are taken: $n = 1.035$, $n = 1.047$ and $n = 1.059$. In Fig. 5 the scattered diagram for $\theta_0 = 0^\circ$ is shown for an erythrocyte shape V1 (max. residual 0.7%). In contrast to the shape influence, the influence of the refractive index on the curves is visible even in the vicinity of the main peak. This influence gets even stronger with increasing values of the incident angle in Figs. 6–8 (max. residual 0.3%). Corresponding results are presented for shape V2 in Figs. 9 and 10 (max. residual 0.7% and 0.4% correspondingly).

In cytometry the exact determination of the volume, shape and refractive index of erythrocyte is of importance. In connection with the results presented above one can conclude that it is useful to measure light scattering over an angle range as wide as possible. Therefore a scanning flow cytometer (SFC) described in [12,14] which allows measuring a wider range of scattering angles seems to be an advantageous tool for the investigations of light scattering by an erythrocyte.

5. Conclusions

In this paper the DSM has been applied to compare light scattering by realistic biconcave shapes of a human erythrocyte. The DSM algorithm has been extended to calculation of shape profiles given numerically and having deep concavities. The new representation for the internal fields providing an increased stability of numerical results has been used. The influences of different shape profiles and the refractive indices of the erythrocyte on light scattering have been

presented. It was found that their influence on the scattered intensity can be observed over a wide angle range. Moreover, a higher refractive index causes a higher level of the scattered intensity in almost whole range of the observation angles. Because of this it seems reasonable for experimental investigations to measure in an as wide scattering angle range as possible to be able to distinguish between erythrocyte parameters. It seems that higher incident angles are more preferable for observations are, as the intensity gives more information about the shape and refractive index. Further investigations in this area are needed to find univocal correspondence between erythrocyte parameters and the measured scattered intensity and help in the future for solving the inverse scattering problem.

Acknowledgments

The author gratefully acknowledges funding of this research by Deutsche Forschungsgemeinschaft (DFG) and the Russian Foundation for Basic Research (RFBR).

References

- [1] Lugovskaja SA, Morosova VT, Pochtar ME, Dolgov VV. Laboratory hematology. Moscow: Labpress; 2002 [in Russian].
- [2] Tarasov P, Yurkin M, Avrorov P, Semyanov KA, Hoekstra A, Maltsev V. Optics of erythrocytes. In: Hoekstra A, Maltsev V, Videen G, editors. Optics of biological particles. Berlin: Springer; 2007.
- [3] Wriedt T, Hellmers J, Eremina E, Schuh R. Light scattering by single erythrocyte: comparison of different methods. *JQSRT* 2006;100(1–3):446–56.
- [4] Eremina E, Eremin Y, Wriedt T. Analysis of light scattering by different shape models of erythrocyte based on discrete sources method. *Opt Commun* 2005;244:15–23.
- [5] Ramm AG. Multidimensional inverse scattering problems. New York: Longman Scientific/Wiley; 1992.
- [6] Maltsev VP, Semyanov KA. Characterisation of bio-particles from light scattering VSP. Boston: Utrecht; 2004.
- [7] Lu JQ, Yang P, Hu XH. Simulations of light scattering from a biconcave red blood cell using the finite-difference time-domain method. *J Biomed Opt* 2005;10(2):024022.
- [8] Yurkin MA, Semyanov KA, Tarasov PA, Chernyshev AV, Hoekstra AG, Maltsev VP. Experimental and theoretical study of light scattering by individual mature red blood cells with scanning flow cytometry and discrete dipole approximation. *Appl Opt* 2005;44(25):5249.
- [9] Nilsson AMK, Alsholm P, Karlsson A, Andersson-Engels S. T-matrix computations of light scattering by red blood cells. *Appl Opt* 1998;3:2735.
- [10] Eremina E, Hellmers J, Eremin Y, Wriedt T. Different shape models for erythrocyte. Light scattering analysis based on the discrete sources method. *JQSRT* 2006;102:3–9.
- [11] Skalak R, Tozeren A, Zarda RP, Chien S. Strain energy factor of red blood cell membranes. *Biophys J* 1973;13:245–64.
- [12] Fung YC, Tsang WC, Patitucci P. High-resolution data on the geometry of red blood cell. *Biorheology* 1981;18:369–85.
- [13] Svetina S, Kuzman D, Waugh RE, Zihel P, Zeks B. The cooperative role of membrane skeleton and bilayer in the mechanical behaviour of red blood cells. *Bioelectrochemistry* 2004;62:107–13.
- [14] Eremin YuA. The method of discrete sources in electromagnetic scattering by axially symmetric structures. *J Commun Technol Electron* 2000;45(2):269.
- [15] Colton D, Kress R. Inverse acoustic and electromagnetic scattering theory. Berlin: Springer; 1992.
- [16] Doicu A, Eremin Yu, Wriedt T. Acoustic and electromagnetic scattering analysis using discrete sources. London: Academic Press; 2000.
- [17] Voevodyn V, Kuznetsov A. Matrices and calculations. Moscow: Science; 1982 [in Russian].
- [18] Maltsev VP. Scanning flow cytometry for individual particle analysis. *Rev Sci Instrum* 2000;71:243.
- [19] Surface evolver code: <<http://www.susqu.edu/brakke/evolver/evolver.html>>.